GeoScienceWorld
Lithosphere
Volume 2022, Article ID 7057344, 19 pages
https://doi.org/10.2113/2022/7057344

Lithosphere

Research Article

Experimental and Field Investigations on the Impact-Resistance Mechanical Properties of Negative Poisson's Ratio Bolt/Cable

Jiong Wang,[1,2] **Peng Liu**,[1,2] **Zimin Ma**,[3] **Manchao He**,[1,2] **Chengzhang Gao**,[4] **and Chun Zhu**[5]

[1]*State Key Laboratory for Geomechanics & Deep Underground Engineering, Beijing 100083, China*
[2]*School of Mechanics and Civil Engineering, China University of Mining & Technology (Beijing), Beijing 100083, China*
[3]*School of Resource and Environmental Engineering, Shandong University of Technology, Zibo 255000, China*
[4]*ShanXiYinFeng S&T Co., Ltd., Shanxi 030000, China*
[5]*School of Earth Sciences and Engineering, Hohai University, Nanjing 210098, China*

Correspondence should be addressed to Peng Liu; liupeng.20131773@gmail.com

Received 23 June 2022; Accepted 4 August 2022; Published 25 August 2022

Academic Editor: Shaofeng Wang

Copyright © 2022 Jiong Wang et al. Exclusive Licensee GeoScienceWorld. Distributed under a Creative Commons Attribution License (CC BY 4.0).

Dynamic impact tests of negative Poisson's ratio (NPR) and rebar bolts under different impact wavelengths were carried out using a self-developed NPR bolt tensile impact test system. Additionally, a field anti-impact test using blasting was performed to simulate rockburst, and the field anti-impact characteristics of the NPR and conventional cable were compared and analysed. The experimental test results revealed that the peak impact force of the NPR and rebar bolts was inversely proportional to the wavelength. The NPR bolt underwent only constant resistance structural deformation, and the rod body did not break. The rebar bolt body fractured and necked. Under the same impact wavelength, the impact force and elongation of the two bolt types were proportional to the impact velocity. Compared with the greater peak impact force of the rebar bolt, the NPR bolt output structure deformation reduced the peak impact force. At the same impact velocity, as the wavelength increased, the impact force of the NPR bolt decreased rapidly, and the number of peaks also decreased. The impact force peak value of the rebar bolt was high, the impact force-time curve had multipeak characteristics, and no apparent rapid attenuation occurred. The field test results indicated that the NPR cable could produce slip deformation under the action of an explosion impact force to absorb the impact energy and that it had special mechanical properties to maintain a constant resistance. Under the same equivalent blasting impact energy, the conventional cable test section collapsed completely. The NPR cable test section was stable overall, verifying that the NPR cable had better impact-resistance mechanical properties than conventional cable. The research results provide a reliable basis for the effectiveness of NPR bolts/cables in preventing rockbursts.

1. Introduction

Shallow resources on Earth are increasingly undergoing depletion owing to mining [1]. In contrast, the mining of deep resources has the characteristics of "four highs and one disturbance," which severely threatens the safety of construction workers [2–4]. Humans have built deep large-scale water diversion tunnels, deep mining projects for nonmetallic and metallic mines, underground water-sealed oil caverns, deep burial and disposal projects for nuclear waste, and so on [5–7]. However, several safety problems have been encountered during the construction phase of these underground projects [8–10]. One of the most severe safety problems is rockburst (Figure 1), which has been defined by Blake [11] as the sudden destruction of rock, characterised by the rupture and protrusion of rock from the surrounding rock and accompanied by a violent release of energy.

The Altenberg tin mine in Germany suffered a rockburst in 1640, severely hindering production [12]. The Leipzig mine in the UK had a recorded rockburst in 1738 [13]. The Atlantic mine in the USA, Karal gold mine in India, Sudber mine in Canada, El Teniente copper mine in Chile, Hegura road tunnel in Norway, and Vestal drinking water tunnel in Sweden have all suffered from rockbursts [14].

Downloaded from http://pubs.geoscienceworld.org/gsa/lithosphere/article-pdf/doi/10.2113/2022/7057344/5681874/7057344.pdf
by guest

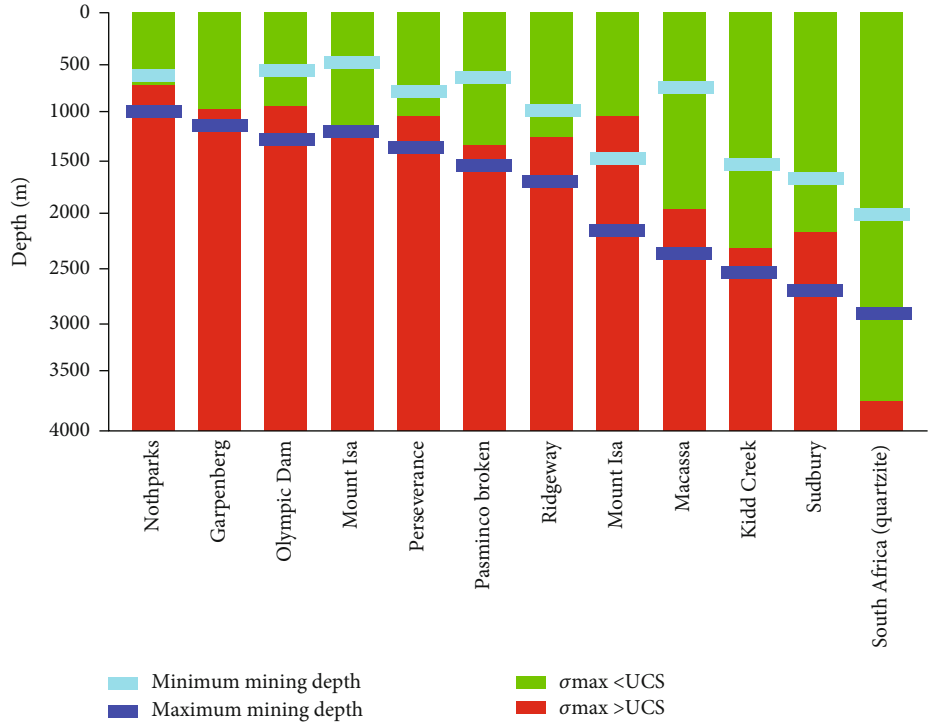

Figure 1: Regularity of stress-strength ratio with mining depth.

As the depth of mining increases, the maximum principal stress increases to or even exceeds the uniaxial compressive strength of the rock, and the probability of rockbursts increases significantly (Figure 1). In China, the earliest recorded rockburst occurred in 1933 at the Fushun Shengli coal mine [14]. A severe rockburst occurred during the construction of a drainage tunnel at the Jinping II hydropower station, burying the TBM machine and killing seven people, posing a severe threat to the lives of workers [15]. In addition, the Hongtushan copper mine, Jinchuan II mine, Dongguashan copper mine, Huize lead-zinc mine, Lingbao Yinxin gold mine, Erdaogou gold mine, Linglong gold mine, Fankou lead-zinc mine, Zhazixi antimony mine, Dahongshan iron ore mine, and Jiguanzui gold mine experienced several slight-strong rockbursts from 1976 to 2015. This posed a long-term threat to the lives of underground workers [16]. In addition, the Bayu Tunnel, the world's first severe rockburst tunnel on a plateau, experienced 94% of rockbursts during construction.

Bolt supports can control the deformation of the surrounding rock and improve its strength. Therefore, it is widely used as an effective method for preventing rockbursts [17]. According to the performance of the supporting materials, bolts can be divided into the following three types [18]: strength, yield, and energy absorption bolts. The supporting resistance of a strength bolt is determined by its material strength. For example, the support resistance of a rebar bolt is equal to the strength of the bolt material. This type of bolt has the characteristics of high strength and small deformation. Yield bolts, such as split sets [19], have the characteristics of a small supporting resistance and large deformation. Satisfying the high-stress impact support requirements is challenging particularly in deep mines [20–23]. In 1995, McCreath and Kaiser proposed design guidelines for energy-absorbing bolts [24]. The most basic requirement of an energy-absorbing bolt is to be able to output 200-300 mm yielding deformation at high strength [25]. The bolt should have sliding characteristics in the structure with the deformation of the surrounding rock, which is primarily applied to underground surrounding rock support engineering affected by instantaneous load [26]. The energy-absorbing bolt has the following characteristics: (1) rebar bolt strength, (2) deformation capacity of the Split set bolts, and (3) rapid response capability to the external load. The main representative bolts are the Garford solid dynamic [27–29], cone [30], MCB cone [31–36], D [37], Roofex, and NPR bolts.

Jager (South Africa, 1992) developed the cone bolt [31]. It absorbs deformation energy through shear-slip, and the rod yields at the conical anchorage end. The maximum support resistance is 200 kN, the allowable tensile amount is 600 mm, and the energy absorption can reach 40-100 kJ. Ansell (Norway, 2006) developed the D bolt [29], which is primarily composed of smooth metal rods and interactive anchoring units and is anchored by a resin or cement anchoring agent during installation. The total length of D bolt is 2.7 m, and the diameter of the rod is 20 mm, which can provide support resistance of 195 kN, maximum deformation of 63 mm (elongation of 18%), and absorbed deformation energy of 74 kJ. The Garford dynamic bolt, developed by Garford (Australia, 2007), is fabricated from a rod body and a thick-threaded steel casing. The supporting force is 100-125 kN, and the maximum allowable deformation is 500 mm [27, 28, 37]. Ozbay and Neugebauer (Australia,

Downloaded from http://pubs.geoscienceworld.org/gsa/lithosphere/article-pdf/doi/10.2113/2022/7057344/5681874/7057344.pdf
by guest

2009) developed the Roofex bolt [38], a structural slip-type bolt with a design resistance (80-90 kN), an elongation of 300 mm, and a tensile capacity proportional to the impact energy. The development and application of these traditional energy-absorbing bolts have contributed to safe mining. However, they are still fabricated from conventional positive Poisson's ratio materials. The relationship between the support working resistance and deformation is the traditional elastic deformation-strain strengthening-strain softening model, and the working resistance varies with the displacement. Therefore, it remains difficult to satisfy the requirements of deep dynamic disaster prevention.

To satisfy the requirement of support in mining engineering, He et al. developed a constant-resistance large-deformation bolt/cable [39, 40]. The core energy-absorbing device exhibits an NPR effect, which is also known as an NPR bolt/cable [41]. The NPR bolt is a new type of energy-absorbing bolt with extraordinary material properties such as continuous tension, high constant resistance, and ideal elastic plasticity. Unlike a typical energy-absorbing bolt, its constant resistance is primarily related to the structural characteristics of the NPR device. It is unrelated to the external load and rock properties [41]. Since the successful development of the NPR bolt, it has been widely used in field mine supports and has achieved excellent results. Additionally, static tensile, drop weight, and physical model tests have been performed, and key parameters such as constant resistance, axial deformation, and expansion of the NPR bolt have been obtained. The NPR structure and energy absorption characteristics were analysed.

The complexity of support design increases when rock masses undergo sudden and violent damage owing to rockbursts and other activities. The study of the dynamic performance of supports has been a popular topic over the last four decades [42, 43]. Sharifzadeh et al. [44] analysed the influence of the dynamic performance of energy-absorbing bolts, classification, and inherent properties on the dynamic performance of bolts based on the results of laboratory tests. Knox et al. [45] studied the relationship between the magnitude of impact velocity and accumulated energy of bolts using a dynamic impact tester (DIT). They concluded that there was no significant change in the cumulative proximal displacement or cumulative maximum energy absorbed by the rock bolt over the range of the impact velocities tested. Although the impact velocity affected the average strain rate during the impact, the change in strain rate resulted in insignificant changes in the impact load. Li and Doucet [46] investigated the dynamics of D bolts with different diameters and lengths. They concluded that the displacement of D bolts increased linearly with the impact energy. Wang et al. [47] investigated the dynamic response of a BHRB400 bolt under various impact scenarios. They classified the yielding phase of the bolt during impact loading into transient and steady-state yielding, with the peak load of transient yielding being significantly higher than the steady-state yielding load.

Existing dynamic performance test facilities are generally based on the mechanical impact principle, where gravitational potential energy is converted into kinetic energy as the impact energy. The test facilities can be divided into two categories. One uses the direct impact method, and the other is based on momentum transfer mechanisms [48]. Deep dynamic load strain rates are primarily in the range 10^1-$10^3\,s^{-1}$ or even higher. This range corresponds to medium and high strain rates [49–53]. In contrast, strain rates are in the range of 10^0-$10^2\,s^{-1}$ for the drop hammer and pendulum experiments. These fall under the category of low-velocity impacts (Figure 2). Representative experimental methods for medium and high strain rate impacts primarily include Hopkinson experiments, which can be divided into two categories: compression and tension bars, with a strain rate range of 10^1-$10^3\,s^{-1}$ [54–56]. Based on this, He improved the Split Hopkinson pressure bar (SHPB) experimental system to form an NPR bolt/cable impact tensile test system.

This study explored the dynamic characteristics of NPR bolts/cables under different impact wavelengths and their field impact protection performance. The NPR bolt impact tensile test system was used to study the dynamic response characteristics of NPR and rebar bolts at three different impact wavelengths (0.6, 1.0, and 1.4 m). The corresponding impact force-time and elongation-time relationships were obtained. The effect of the impact wavelength on the dynamic response characteristics of the NPR and rebar bolts was clarified. Additionally, a field impact test was performed to compare the impact resistance of NPR and conventional cables by arranging the blasting source parallel to the roadway alignment to simulate a rockburst.

2. Experimental Methodology

2.1. NPR Bolt. Based on finite deformation control theory, He et al. proposed an NPR bolt/cable with near-ideal elasto-plastic properties, which can achieve large deformations under constant resistance [41]. The NPR bolt consists of a rod, sleeve, cone, plate, and nut (Figure 3). In particular, the constant-resistance body includes a sleeve and a cone. The cone is rounded, the large end of the cone faces to the right, and the diameter of the large end is slightly larger than the inner diameter of the sleeve by 2 mm. The small end of the cone faces to the left, and the diameter of the small end is the same as that of the rod. This structure of the NPR bolt transforms most of the material deformation of the bolt into structural deformation; the constant resistance of the NPR bolt is not related to the external load but only to the elastic parameters of the sleeve and structural dimensions of the rod. The constant design resistance of the NPR bolt is 80-90% of the yield strength of the rod to ensure that the rod is in an elastic working condition during operation. The material strength of the sleeve is lower than that of the body, which ensures that friction failure of the constant-resistance structure does not occur. When the NPR bolt is operating, the left side of the rod is anchored in stable rock with a resin coil as the anchor end, and the right side of the constant-resistance sleeve is fixed to the outside of the rock with a nut and tray. When the external load is less than the constant resistance of the NPR bolt, it resists the external load via elastic deformation. When the external load reaches the constant resistance of the NPR bolt, it is in ultimate equilibrium. When the external load continues to increase, the sleeve of the NPR bolt begins to move in the direction of

Downloaded from http://pubs.geoscienceworld.org/gsa/lithosphere/article-pdf/doi/10.2113/2022/7057344/5681874/7057344.pdf
by guest

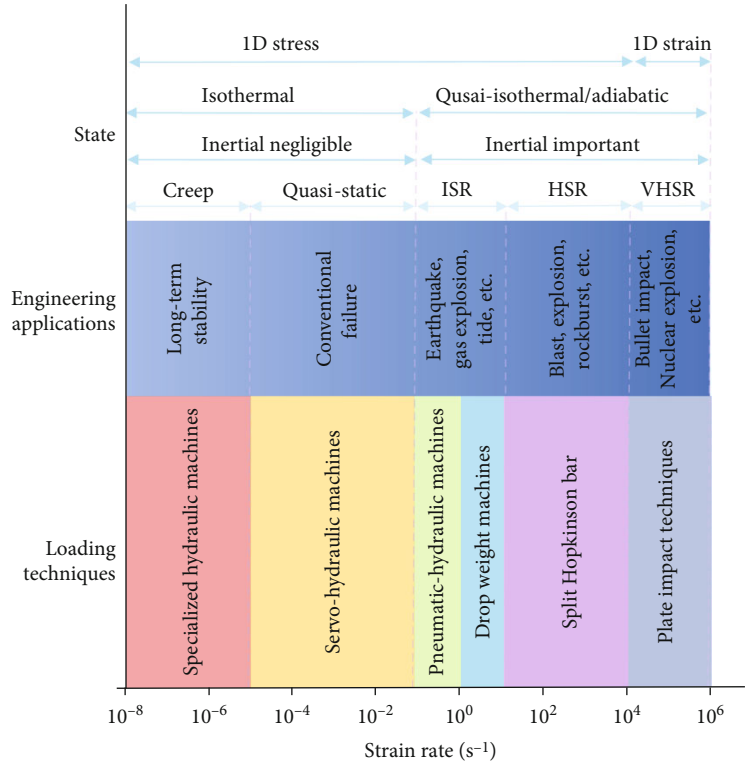

Figure 2: Relationship of loading techniques and strain rates (modified after Zhou et al.; Zhang et al.) [54, 57].

the external load, and this displacement is the axial deformation of the NPR bolt. The working resistance of the NPR bolt originates from the friction between the cone and sleeve under an external load. Because the contact area between the cone and sleeve remains constant, the kinetic friction between them remains constant, and the working resistance of the NPR bolt remains relatively constant. The constant resistance of the NPR bolt selected for the test was 130 kN.

2.2. Experimental Apparatus. The experimental system consisted of an SHPB dynamic loading system, bolt impact tension system, and data acquisition system (Figure 4). According to the different experimental requirements and research objects, the bolt impact tensioning system was divided into NPR and rebar bolt impact tensioning systems to conduct dynamic impact experiments on rebar and NPR bolts for comparison. We studied and verified the dynamic mechanical properties of various bolt types under impact.

2.2.1. SHPB Dynamic Loading System. The dynamic loading system is shown in Figures 4(a) and 4(b). High-pressure nitrogen gas from the main cylinder entered the chamber and propelled the bullet through the chamber at a set gas strength. After the bullet passed through the relief hole at the end of the chamber, nitrogen gas was released into the air to relieve pressure. The bullet travelled at a constant speed through the chamber for a certain distance before exiting the chamber and striking the entry sleeve, completing the loading of the anchor specimen. The chamber was fabricated from high-strength steel and was 30 mm thick.

The leading performance indicators of the Hopkinson dynamic loading system were as follows:

(1) Controller basic size: 700 mm × 700 mm × 1500 mm (length × width × height)

(2) Gun chamber system length: 3950 mm

(3) Nitrogen cylinder: volume was 6 m^3; nitrogen purity ≥ 99.5% (V/V); oxygen content ≤ 0.5% (V/V); moisture < 100 mL/bottle; maximum pressure 15.0 ± 0.5 MPa (20°C)

(4) Main pressure valve pressure loading range: 0-25 MPa

(5) Subpressure valve pressure-loading range: 0-6 MPa

The bullets used in the experiments were 35CrMn steel with a diameter of 75 mm and lengths of 300, 500, and 700 mm. According to the stress wave theory, the wavelength can be calculated by $\lambda = 2L$, where L is the length of the bullet. So the corresponding wavelength is 0.6, 1.0, and 1.4 m, respectively.

2.2.2. Impact Tensile Experimental System. A schematic of the bolt impact tensile test system is shown in Figure 4(b). It was composed of an incident rod, guide frame, sample fixed support, connection screw, bolt sample, nut, and composite bearing tray. The impact sleeve length, diameter, and wall thickness were 2000, 140, and 33 mm, respectively. Both sides of the impact sleeve were tightly bonded with a 140 mm disc with a thickness of 30 mm.

Downloaded from http://pubs.geoscienceworld.org/gsa/lithosphere/article-pdf/doi/10.2113/2022/7057344/5681874/7057344.pdf
by guest

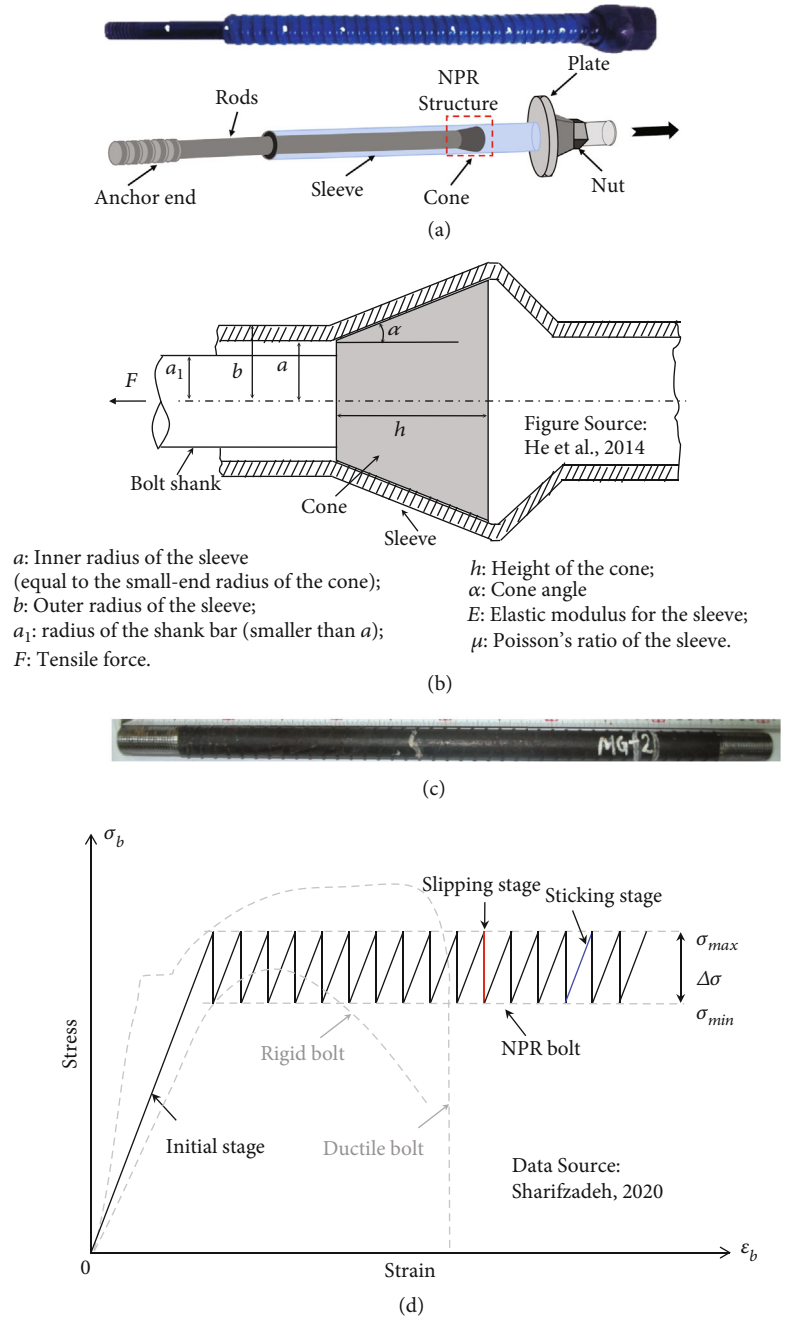

Figure 3: Characteristics of bolts: (a) NPR bolt, (b) NPR structure, (c) rebar bolt, and (d) stress-strain curves of bolts.

2.2.3. Data Acquisition System. The data acquisition system consisted of three main components: a laser velocimetry system, impact force measurement system, and laser displacement monitoring system (Figure 4(c)). The laser velocimetry system was installed at the end of the chamber, with two laser sensors at the upper end, which emitted two laser beams at a distance of 20 mm vertically downward. After passing through the chamber vent, the bullet moved at a constant speed and passed through the two laser beams, interrupted by the two laser sensors. The precise time interval between the two laser beams being interrupted was equal to the time of the bullet passing through the 20 mm distance, thus enabling the speed of the bullet movement to be calculated.

The impact measurement system consisted of a composite carrier tray, a 24-bit INV3020C high-precision data acquisition instrument, 24-bit INV3020C high-precision data acquisition instrument, INV1870 (DLF-4) charge amplifier, DASP-V10 test analysis software, and three dynamic BLA-2A piezoelectric sensors.

3. Experimental Results and Interpretations

3.1. Testing Scheme. The dynamic response characteristics of the bolt were different under different wavelengths and impact velocities. Therefore, during this test, we considered three wavelengths and four impact velocities, resulting in a

Downloaded from http://pubs.geoscienceworld.org/gsa/lithosphere/article-pdf/doi/10.2113/2022/7057344/5681874/7057344.pdf
by guest

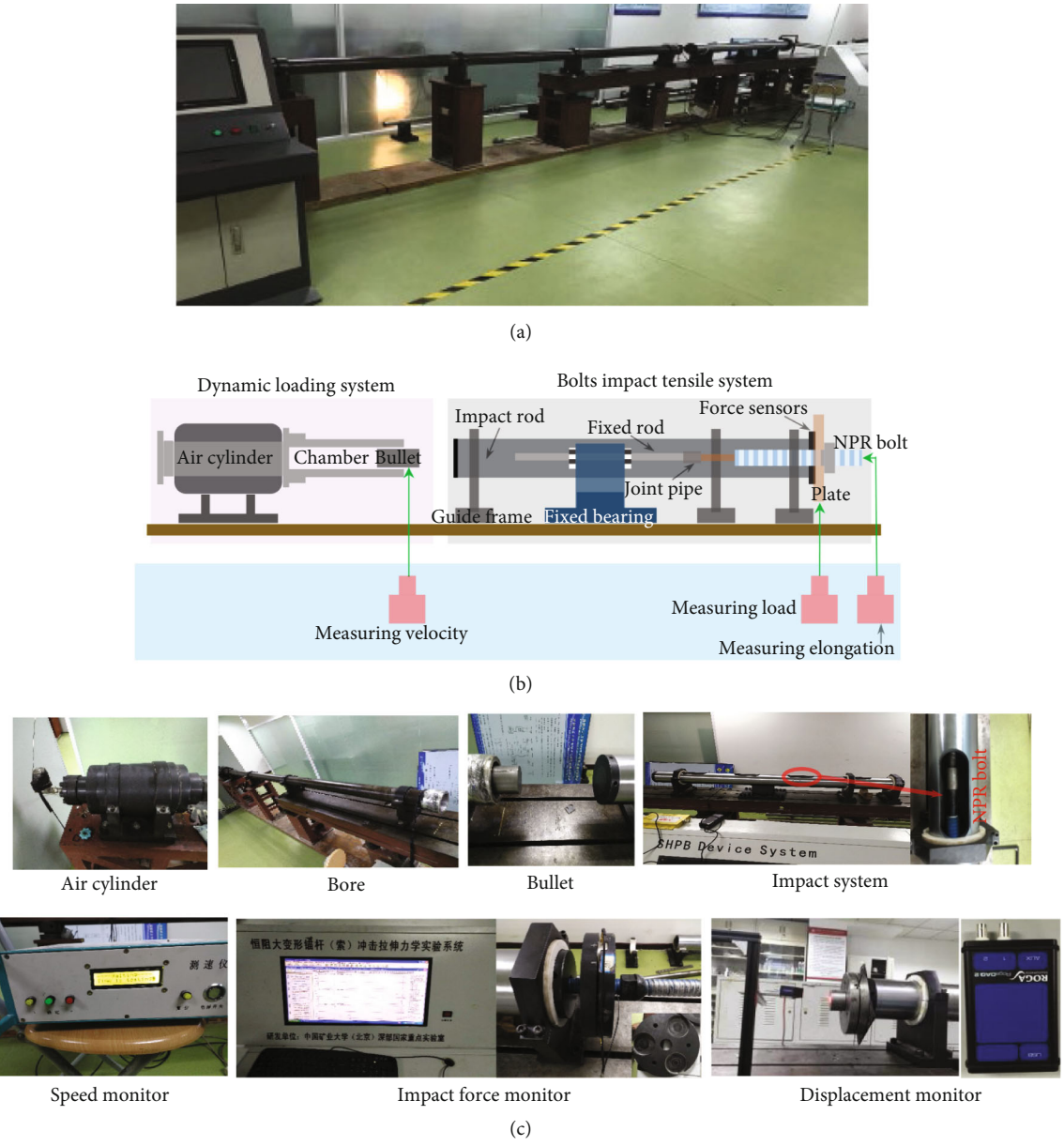

Figure 4: Experimental setup: (a) NPR bolt impact tensile test system, (b) schematic view, and (c) experimental instruments.

total of 12 test schemes (Table 1). In the NPR impact tensile test, the bullet length reflected the wavelength, and the gas pressure reflected the impact velocity. A laser velocimeter was used to measure the impact velocity of each specification bullet at each gas pressure. In the experiment, a data acquisition device collected the bullet impact velocity, impact force-time history curve, and displacement time history curve.

3.2. Experimental Phenomena. The impact test results for the NPR and rebar bolts are shown in Figure 5. The NPR bolts were flushed entirely out after average 71 impacts. The rebar bolts fractured suddenly at average 15impacts, and no noticeable sign was observed before fracturing. The rebar bolt exhibited no apparent elongation after each impact until there was no sign of "brittle fracturing." The NPR bolt exhibited noticeable elongation during the impact process and did not undergo brittle fracturing.

3.3. Wavelength of 0.6 m

3.3.1. Gas Pressure of 1.0 MPa. When the shock wavelength was 0.6 m, the impact velocity was 14.58 m/s. The impact force of the NPR bolt reached a maximum peak value of 315.31 kN at 0.25 ms and a second peak value of 221.67 kN at 1.76 ms, and the impact force action time was approximately 5.00 ms (Figure 6). The NPR bolt reached the maximum elongation of 13.35 mm at 7.11 ms and gradually reduced the rebound. The maximum negative elongation was -7.35 mm at 23.99 ms, and the rebound was deformed again. Finally, after approximately 60 ms, the elongation recovered to 0.05 mm (Figure 7).

Downloaded from http://pubs.geoscienceworld.org/gsa/lithosphere/article-pdf/doi/10.2113/2022/7057344/5681874/7057344.pdf
by guest

Table 1: Impact test scheme.

Sample number	Wavelength (m)	Gas pressure (MPa)	Impact velocity (m/s)
NPR-1/R-1	0.6	1.0	14.58
NPR-2/R-2		1.5	17.52
NPR-3/R-3		2.0	18.79
NPR-4/R-4		2.5	22.85
NPR-5/R-5	1.0	1.0	12.12
NPR-6/R-6		1.5	15.42
NPR-7/R-7		2.0	17.21
NPR-8/R-8		2.5	19.01
NPR-9/R-9	1.4	1.0	9.56
NPR-10/R-10		1.5	12.67
NPR-11/R-11		2.0	13.69
NPR-12/R-12		2.5	16.05

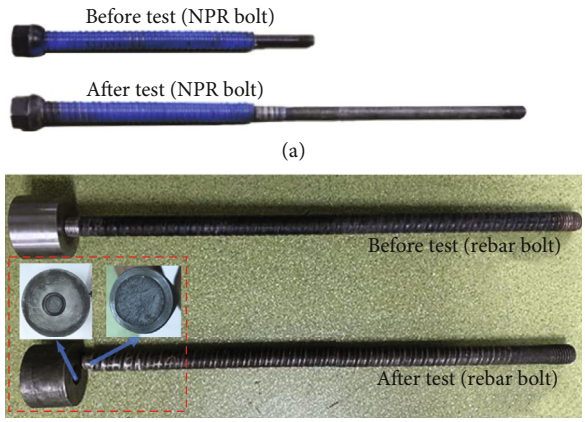

Figure 5: Photos of NPR and rebar bolt before and after test.

The impact force of the rebar bolt reached a maximum peak of 329.09 kN at 0.21 ms and a second peak of 296.29 kN at 2.03 ms, and the impact force action time was approximately 6.23 ms (Figure 6). The rebar bolt reached a maximum elongation of 14.47 mm at 4.61 ms and then gradually reduced the rebound; the corresponding maximum negative elongation was -3.55 mm at 13.81 ms, after which the bolt deformed again. After approximately 40.00 ms, the elongation recovered to 0 (Figure 7).

3.3.2. Gas Pressure of 1.5 MPa. The impact force of the NPR bolt reached a maximum peak of 447.72 kN at 0.21 ms and a second peak of 341.06 kN at 1.67 ms, and the impact force action time was approximately 4.35 ms (Figure 6). The NPR bolt reached the maximum elongation of 18.89 mm at 5.40 ms and gradually reduced the spring back. A negative maximum elongation of -4.72 mm was produced at 20.31 ms and then deformed again. After approximately 50.00 ms, elongation was stable at approximately 2.23 mm (Figure 7).

The impact force of the rebar bolt reached a maximum peak of 466.54 kN at 0.23 ms and a second peak of 337.58 kN at 1.45 ms, and the impact force action time was approximately 3.67 ms (Figure 6). The rebar bolt reached a maximum elongation of 16.80 mm at 4.00 ms and gradually reduced the rebound. At 13.62 ms, the maximum negative elongation was -2.94 mm, and the rebound was deformed again. Finally, after approximately 30.00 ms, the elongation recovered to 0 (Figure 7).

3.3.3. Gas Pressure of 2.0 MPa. The impact force of the NPR bolt reached a maximum peak of 540.3 kN at 0.31 ms and a second peak of 369.20 kN at 3.93 ms, and the impact force action time was approximately 7.00 ms (Figure 6). The NPR bolt reached a maximum elongation of 24.13 mm at 5.35 ms and gradually reduced the spring back. A negative maximum elongation of -5.91 mm was produced at 14.97 ms and then deformed again. After approximately 30.00 ms, elongation was stable at approximately 3.16 mm (Figure 7).

The impact force of the rebar bolt reached a maximum peak value of 604.94 kN at 0.30 ms, whereas the second peak value reached 517.49 kN at 2.10 ms, and the impact force action time was approximately 5.46 ms (Figure 6). The rebar bolt reached the maximum elongation of 17.80 mm at 4.10 ms and gradually reduced the rebound. A maximum negative elongation of -5.34 mm was generated at 15.39 ms, and the deformation rebounded again. Finally, after approximately 70 ms, the elongation recovered to 0 (Figure 7).

3.3.4. Gas Pressure of 2.5 MPa. The impact force of the NPR bolt reached a maximum peak of 644.55 kN at 0.26 ms and a second peak of 551.27 kN at 2.43 ms, and the impact force action time was approximately 7.60 ms (Figure 6). The NPR bolt reached a maximum elongation of 23.17 mm at 8.53 ms and then gradually reduced the rebound, and the minimum elongation was 5.02 mm at 43.77 ms. Finally, after approximately 80 ms, the elongation was stable at 9.72 mm (Figure 7).

The impact force of the rebar bolt reached a maximum peak of 693.22 kN at 0.24 ms and a second peak of 687.14 kN at 2.00 ms, and the impact force action time was approximately 5.30 ms (Figure 6). The rebar bolt reached a maximum elongation of 24.03 mm at 5.90 ms, gradually reducing the rebound. At 34.78 ms, the maximum negative elongation was -6.25 mm, and the rebound was deformed again. Finally, after approximately 55 ms, the elongation recovered to 0 (Figure 7).

3.4. Wavelength of 1.0 m

3.4.1. Gas Pressure of 1.0 MPa. The impact velocity was 12.12 m/s at the impact wavelength $\lambda = 1.0$ m. The NPR bolt reached a maximum impact force of 236.15 kN at 0.25 ms and a second peak of 188.37 kN at 5.18 ms, with an impact time of approximately 11.40 ms (Figure 8). The NPR bolt reached a maximum elongation of 11.45 mm at 9.15 ms, then gradually decreased in rebound and produced a maximum negative elongation of -3.26 mm at 32.44 ms, after which it

Downloaded from http://pubs.geoscienceworld.org/gsa/lithosphere/article-pdf/doi/10.2113/2022/7057344/5681874/7057344.pdf
by guest

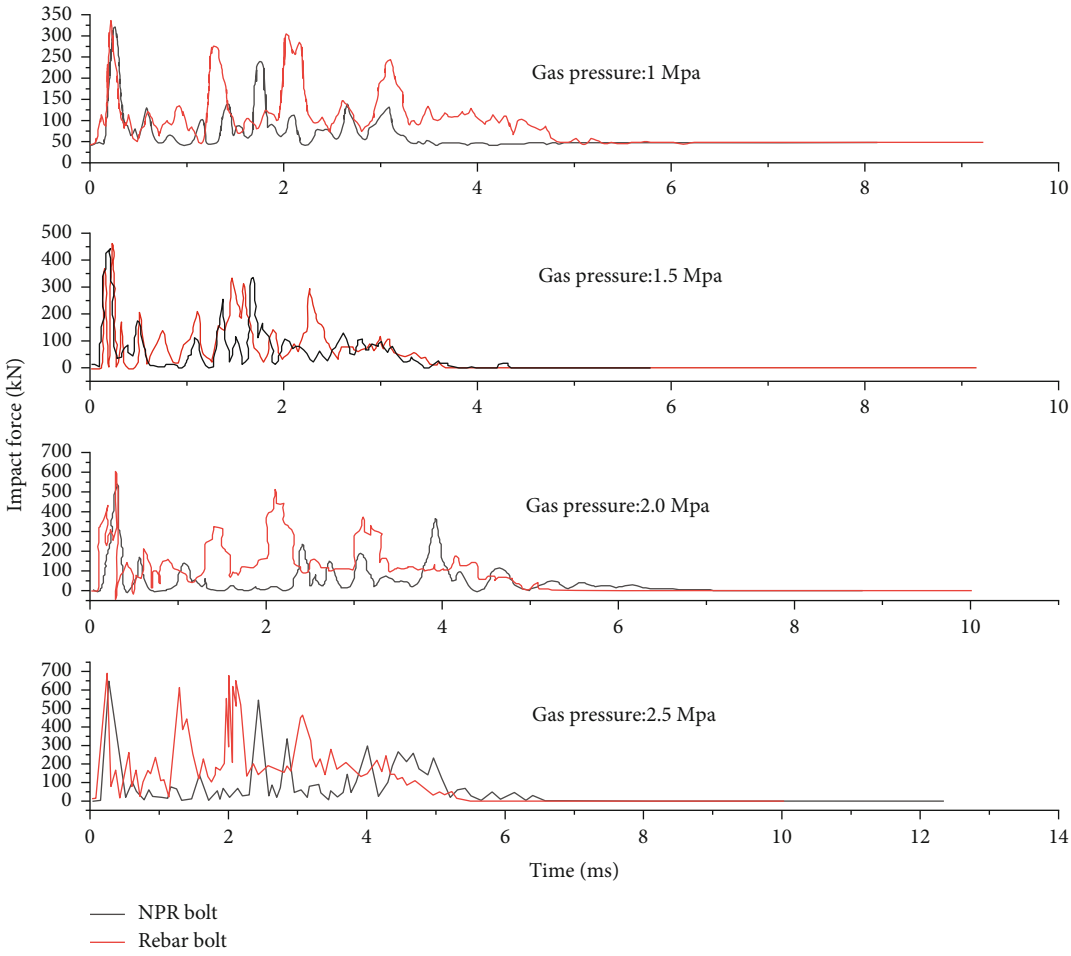

Figure 6: Impact force-time curve for NPR and rebar bolt during impact process (wavelength: 0.6 m).

again deformed and rebounded, eventually returning to 0.07 mm after approximately 50 ms (Figure 9).

The impact force of the rebar bolt reached a maximum peak of 251.39 kN at 0.19 ms and a second peak of 222.56 kN at 2.03 ms, with an impact time of approximately 5.33 ms (Figure 8). The rebar bolt reached a maximum elongation of 14.84 mm at 3.87 ms, then gradually decreased in rebound and produced a maximum negative elongation of -1.35 mm at 13.22 ms, then deformed and rebounded again, eventually returning to 0 mm after approximately 46.62 ms (Figure 9).

3.4.2. Gas Pressure of 1.5 MPa. The impact force of the NPR bolt reached a maximum peak of 417.05 kN at 0.21 ms and a second peak of 394.74 kN at 2.48 ms, and the impact force action time was approximately 5.4 ms (Figure 8). The NPR bolt reached a maximum elongation of 17.25 mm at 5.52 ms and then gradually reduced the rebound. The maximum negative elongation was -4.26 mm at 20.01 ms, and the rebound was deformed again. Finally, after approximately 50 ms, the elongation stabilised at approximately 1.48 mm (Figure 9).

The impact force of the rebar bolt reached a maximum peak of 456.78 kN at 0.28 ms and a second peak of 403.20 kN at 2.05 ms, and the impact force action time was approximately 6 ms (Figure 8). The rebar bolt reached a maximum elongation of 16.17 mm at 3.56 ms, gradually reducing the rebound. The maximum negative elongation was -2.52 mm at 13.31 ms, and the rebound was deformed again. Finally, after approximately 30 ms, the elongation recovered to 0 (Figure 9).

3.4.3. Gas Pressure of 2.0 MPa. The impact force of the NPR bolt reached a maximum peak of 520.09 kN at 0.28 ms and a second peak at 352.85 kN at 2.57 ms, and the impact force action time was approximately 6 ms (Figure 8). The NPR bolt reached the maximum elongation of 20.52 mm at 8.69 ms and gradually reduced the spring back. A negative maximum elongation of -6.21 mm was produced at 29.74 ms and then deformed again. After approximately 50 ms, elongation was stable at approximately 3.22 mm (Figure 9).

The impact force of the rebar bolt reached a maximum peak of 557.16 kN at 0.14 ms and a second peak of 415.46 kN in 1.72 ms, and the impact force action time was approximately 4.34 ms (Figure 8). The rebar bolt reached the maximum elongation of 17.56 mm at 5.45 ms, gradually reducing the rebound. A maximum negative elongation of

Downloaded from http://pubs.geoscienceworld.org/gsa/lithosphere/article-pdf/doi/10.2113/2022/7057344/5681874/7057344.pdf
by guest

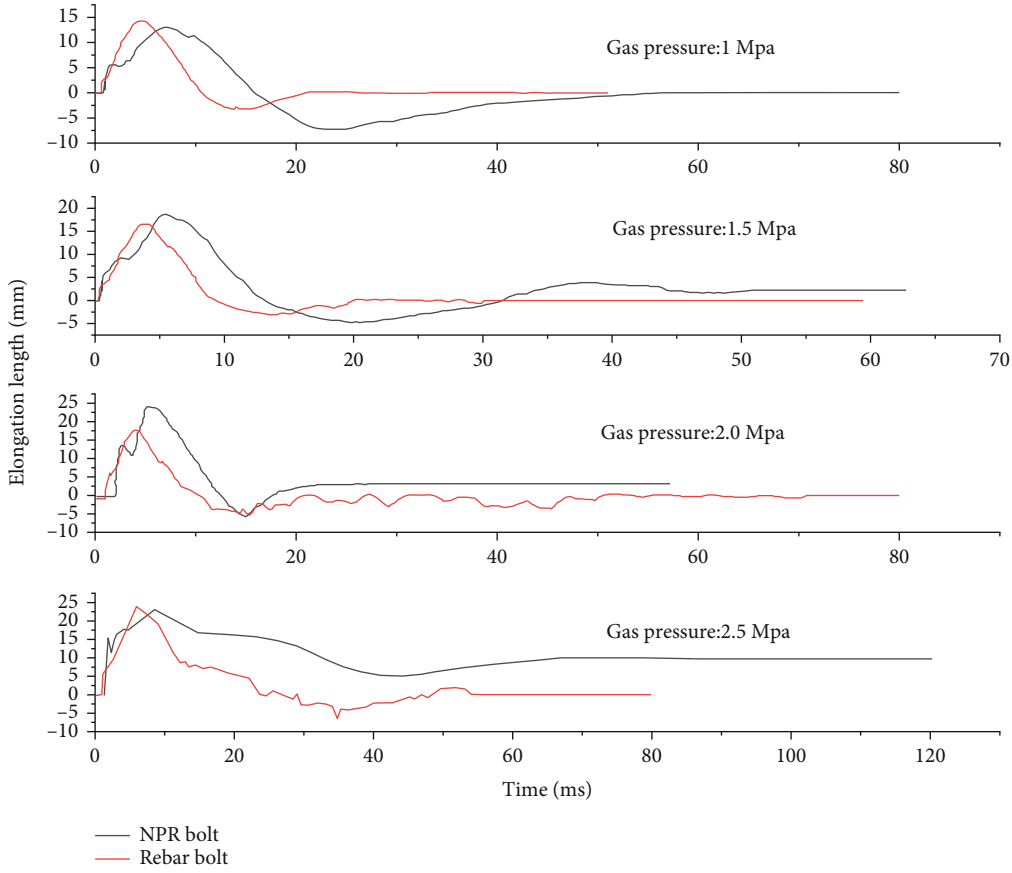

Figure 7: Elongation length-time curve for NPR and rebar bolt during impact process (wavelength: 0.6 m).

-3.90 mm was generated at 38.09 ms, and the rebound was deformed again. Finally, after approximately 28.57 ms, the elongation recovered to 0 (Figure 9).

3.4.4. Gas Pressure of 2.5 MPa. The impact force of the NPR bolt reached a maximum peak of 629.66 kN at 0.25 ms and a second peak of 526.99 kN at 3.35 ms, and the impact force action time was approximately 8.50 ms (Figure 8). The NPR bolt reached the maximum elongation of 22.78 mm at 9.02 ms and then gradually reduced the rebound, and the minimum elongation was 4.46 mm at 43.46 ms. Finally, after approximately 70 ms, the elongation was stable at 7.91 mm (Figure 9).

The impact force of the rebar bolt reached a maximum peak of 673.38 kN at 0.28 ms and a second peak at 458.56 kN at 2.74 ms, and the impact force action time was approximately 5.00 ms (Figure 8). The rebar bolt reached the maximum elongation of 21.67 mm at 5.93 ms and then gradually reduced the rebound. A maximum negative elongation of -7.64 mm was generated at 31.94 ms, and the rebound was deformed again. Finally, after approximately 52.87 ms, the elongation recovered to 0 (Figure 9).

3.5. Wavelength of 1.4 m

3.5.1. Gas Pressure of 1.0 MPa. When the impact wavelength was 1.4 m, the impact velocity was 9.56 m/s. The impact force of the NPR bolt reached the maximum peak of 156.88 kN at 0.38 ms and a second peak of 127.09 kN at 5.00 ms, and the impact force action time was approximately 11.40 ms (Figure 10). The NPR bolt reached the maximum elongation of 3.89 mm at 11.55 ms and gradually reduced the spring back. A negative maximum elongation of -0.86 mm was produced at 34.44 ms and then deformed again. Finally, after approximately 47.57 ms, elongation was restored to 0.07 mm (Figure 11).

The impact force of the rebar bolt reached the maximum peak of 198.38 kN at 0.29 ms and a second peak of 145.79 kN at 3.36 ms, and the impact force action time was approximately 6.14 ms (Figure 10). The rebar bolt reached the maximum elongation of 7.54 mm at 4.99 ms and gradually reduced the rebound. A maximum negative elongation of -1.28 mm was generated at 17.58 ms, and the rebound was deformed again. Finally, after approximately 58.71 ms, the elongation recovered to 0 (Figure 11).

3.5.2. Gas Pressure Equal to 1.5 MPa. The impact force of the NPR bolt reached a maximum peak of 355.00 kN at 0.32 ms and a second peak of 332.70 kN at 3.24 ms, and the impact force action time was approximately 7.79 ms (Figure 10). The NPR bolt reached the maximum elongation of 11.39 mm at 9.21 ms and gradually reduced the spring back. A maximum negative elongation of -2.84 mm was produced at 35.08 ms and then deformed again. After approximately 80 ms, the elongation remained stable at approximately 0.82 mm (Figure 11).

Downloaded from http://pubs.geoscienceworld.org/gsa/lithosphere/article-pdf/doi/10.2113/2022/7057344/5681874/7057344.pdf
by guest

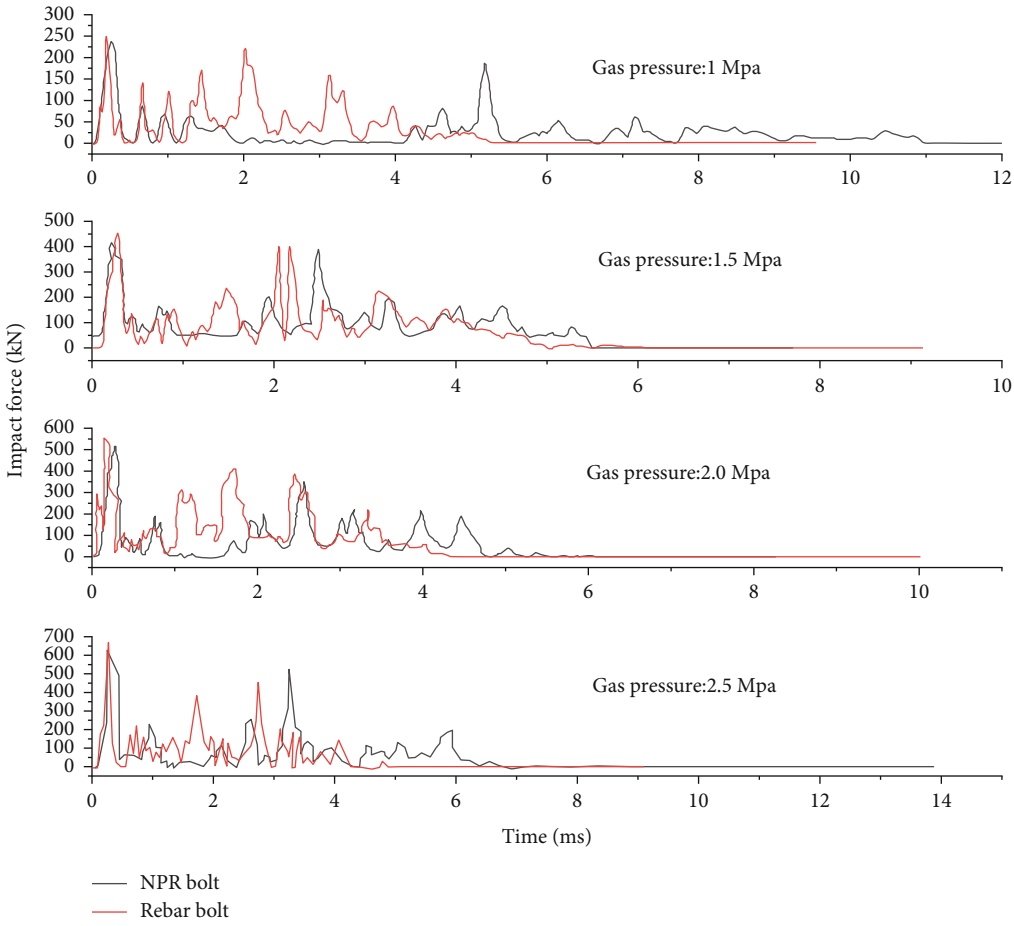

Figure 8: Impact force-time curve for NPR and rebar bolt during impact process (wavelength: 1.0 m).

The impact force of the rebar bolt reached a maximum peak of 435.87 kN at 0.21 ms and reached the second peak of 397.53 kN at 3.23 ms, and the impact force action time was approximately 5.23 ms (Figure 10). The ordinary bolt reached the maximum elongation of 12.74 mm at 2.85 ms and gradually reduced the rebound. The maximum negative elongation of -1.69 mm was generated at 15.70 ms, and the rebound was deformed again. Finally, after approximately 21.00 ms, the elongation recovered to 0 (Figure 11).

3.5.3. Gas Pressure Equal to 2.0 MPa. The impact force of the NPR bolt reached a maximum peak of 498.67 kN at 0.25 ms and reached the second peak of 408.05 kN at 3.23 ms, and the impact force action time was approximately 8.53 ms (Figure 10). The NPR bolt reached the maximum elongation of 13.80 mm at 10.73 ms, gradually reducing the rebound. The maximum negative elongation was -1.64 mm at 55.18 ms. Finally, the elongation was stabilised at approximately 2.57 mm after approximately 98.89 ms (Figure 11).

The impact force of the rebar bolt reached a maximum peak of 524.21 kN at 0.28 ms and a second peak at 442.65 kN at 2.11 ms, and the impact force action time was approximately 5.36 ms (Figure 10). The rebar bolt reached a maximum elongation of 13.43 mm at 5.46 ms and then gradually reduced the rebound. A maximum negative elongation of -1.93 mm was generated at 18.06 ms, and the rebound was deformed again. Finally, after approximately 40 ms, the elongation recovered to 0 (Figure 11).

3.5.4. Gas Pressure of 2.5 MPa. The impact force of the NPR bolt reached a maximum peak of 615.15 kN at 0.33 ms and a second peak of 441.76 kN at 4.22 ms, and the impact force action time was approximately 8.33 ms (Figure 10). The NPR bolt reached a maximum elongation of 15.98 mm at 8.94 ms and then gradually reduced the rebound, and the minimum elongation was 3.16 mm at 42.28 ms. Finally, after approximately 66.54 ms, the elongation was stable at 6.72 mm (Figure 11).

The impact force of the rebar bolt reached a maximum peak of 670.91 kN at 0.54 ms and a second peak of 456.97 kN at 6.71 ms, and the impact force action time was approximately 10.41 ms (Figure 10). The rebar bolt reached a maximum elongation of 18.77 mm at 13.89 ms and gradually reduced the rebound. At 50.10 ms, the maximum negative elongation was -2.53 mm, and the rebound was deformed again. Finally, after approximately 80 ms, the elongation recovered to 0 (Figure 11).

3.6. Comparison Analysis. The impact force was observed to be inversely proportional to the wavelength under the same gas pressure (Figures 6–11) for both the NPR and rebar bolts. The shorter the wavelength, the faster the impact

Downloaded from http://pubs.geoscienceworld.org/gsa/lithosphere/article-pdf/doi/10.2113/2022/7057344/5681874/7057344.pdf
by guest

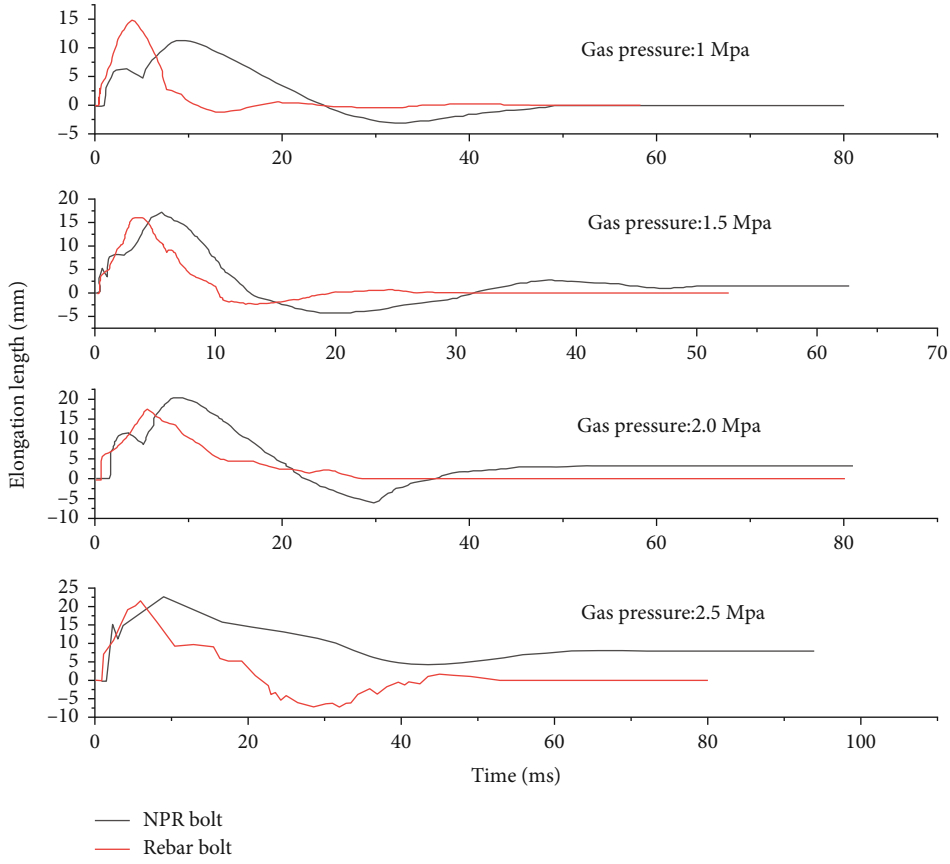

Figure 9: Elongation length-time curve for NPR and rebar bolt during impact process (wavelength: 1.0 m).

speed and the higher the peak impact force. The maximum elongation of the bolt during the impact process was inversely proportional to the wavelength. The shorter the wavelength, the greater the peak value of elongation, and the greater the amplitude of elongation and rebound.

During the impact test, the impact force of the NPR bolt decayed rapidly. After the maximum value appeared, the number of subsequent peaks and the peak values was small. The maximum impact force of the rebar bolt was more prominent, and the curve exhibited a multipeak phenomenon in the impact force response process without apparent rapid attenuation. The results indicated that the NPR bolt can absorb energy rapidly and reduce the impact force. At the same shock wavelength, the peak value of the impact force of the NPR bolt was relatively small, which indicated that the unique stick-slip structure of the NPR bolt can form a buffer effect under an impact load such that the NPR bolt produces structural deformation. The deformation energy of the surrounding rock is absorbed, which can alleviate the instantaneous impact, protect the safety of the roadway, and fully reflect the excellent anti-impact characteristics of the NPR bolt.

In addition, the second wave peak in the impact force-time curve was formed by the impact of the incident rod on the rebound of the bolt and pallet. In the tensile impact experiment of the NPR bolt, under the impact of the bullet, the incident rod formed the first contact with the tray, which was in close contact to generate an impact load, and the bolt began to move while the incident rod was static. When the bolt entered the elastic recovery process, the tray and incident rod impacted again, forming a second peak.

4. Field Investigation

4.1. Engineering Background. Hongyang No. 3 Mine is located in Shenyang City, Liaoning Province (Figure 12). The minefield strike is 5 km long, the east-west width is 6 km, and the area is 28.26 km^2. The mining depth is more than 1000 m. The 707 working face is an isolated island. A rock burst under the influence of dynamic pressure occurred in the roadway. During the excavation of the 1204 working face haulage way (buried depth is more than 1000 m), a strain rock burst occurred, and the rock was thrown up to 27 m. With the increase in the mining depth, the frequency of rockbursts during deep roadway excavation and mining has increased, thereby complicating the process of mining and severely affecting the safety of production.

4.2. Impact Resistance Experimental Design. This field test used the blasting method to simulate the rockburst. The test was selected in 1213 return air roadway (the average buried depth is 805 m), with a test site layout of four sections, each with a length of 10 m. Two sections were conventional cable-reinforced supports and two were NPR cable-reinforced supports (Figure 13). Each test section was reinforced with anchor cable according to design requirements.

Downloaded from http://pubs.geoscienceworld.org/gsa/lithosphere/article-pdf/doi/10.2113/2022/7057344/5681874/7057344.pdf
by guest

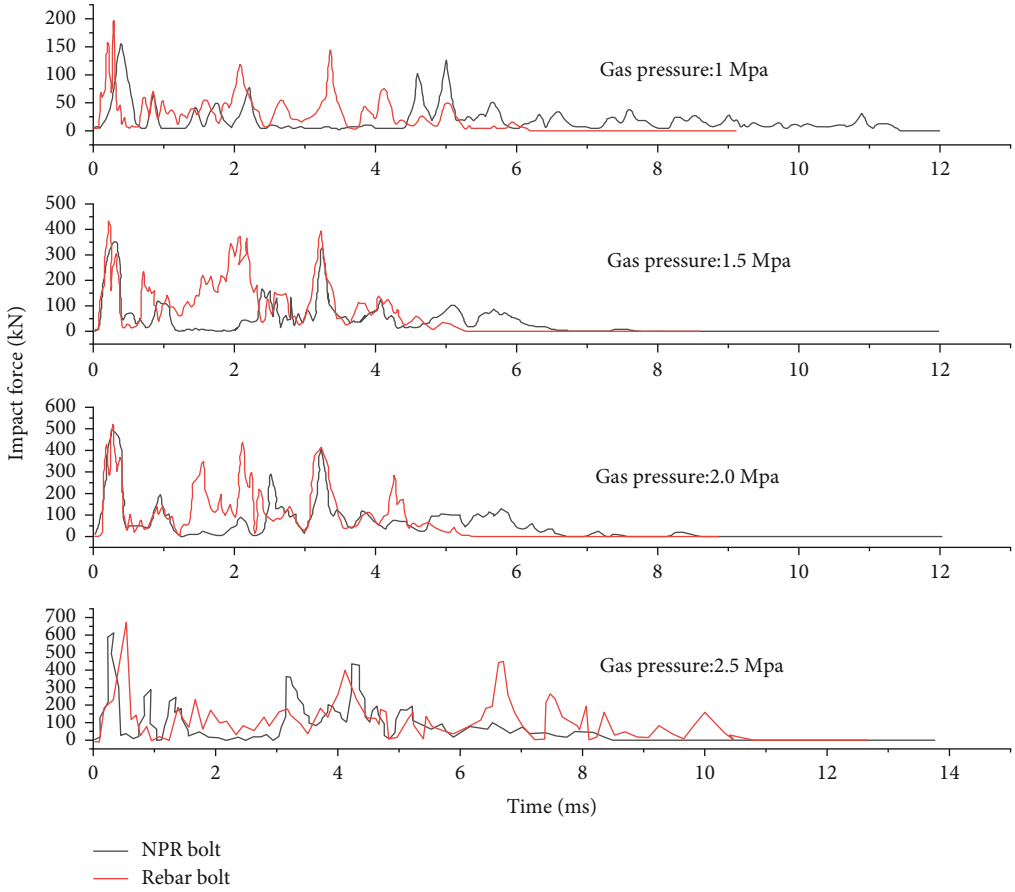

Figure 10: Impact force-time curve for NPR and rebar bolt during impact process (wavelength: 1.4 m).

Subsequently, a blasting chamber was constructed, blast holes were drilled in the roadway direction, and mining emulsion explosives were used to perform the impact tests in the sections. Simultaneously, the cables were dynamically monitored for deformation during the experiments using a remote real-time automatic monitoring technology.

4.2.1. Test Roadway Reinforcement Support. The test section was 108-148 m from the roadway entrance (Figure 12). The roadway was a rectangular section (length: 4200 mm, width: 2500 mm). The bolts and cables were used in original support scheme. Six φ20 mm × 2200 mm strength bolts were installed on the roof, with row and column spacings of 700 and 800 mm, respectively. Eight φ20 mm × 2200 mm strength bolts were installed on the sides, with row and column spacings of 600 and 800 mm, respectively. Two cables with φ21.7 mm × 6500 mm steel strands were installed on the roof. According to the field test requirements, the test section was first strengthened (Figure 13).

(1) Test Sections No. 1 and 4. Conventional cable (φ21.7 mm × 6500 mm steel strand) reinforced support. Each row on the left side of the roadway was arranged using three conventional cables with lengths of 6500 mm. The lowermost cable was 500 mm from the floor, the upper cable was 400 mm from the roof, and the distance between the cables was 800 mm × 1600 mm.

(2) Test Sections No. 2 and 3. NPR cable support (constant resistance force is 350 kN). Three NPR cables with lengths of 6500 mm were arranged in each row on the left side of the roadway, and the preload was 30 t. The roof and right-side supports were unchanged. The lowermost cable was located 500 mm from the floor. The upper cable was placed 400 mm away from the roof. The row and column spacing between the cables was 800 × 1600 mm.

4.2.2. Blasting Chamber Design. Currently, the rockburst in the underground roadway of a coal mine is mostly in 2-3 level, and the corresponding released energy is 106.45-107.8 J. 3# emulsion explosive for mining explosion energy is 2.95 × 106 J/kg [58, 59]. This test used a single blasting for a 10 kg 3# emulsion explosive to simulate the energy of a grade three earthquake.

In this experiment, the blasting source was arranged along the roadway direction to simulate the effect of the shock waves on the roadway support system when a rockburst occurs. The blasting hole was set parallel to the roadway direction, and the chamber was set on the left side of the roadway. Four test sections (no. 1-4) were set, and blasting chambers were formed between test sections no. 1 and no. 2 and between test sections no. 3-no. 4. The distance between the no. 1 blasting chamber and the outside of the test roadway was 138 m. The distance between the no. 2 blasting chamber and the outside was 118 m. The chamber

Downloaded from http://pubs.geoscienceworld.org/gsa/lithosphere/article-pdf/doi/10.2113/2022/7057344/5681874/7057344.pdf
by guest

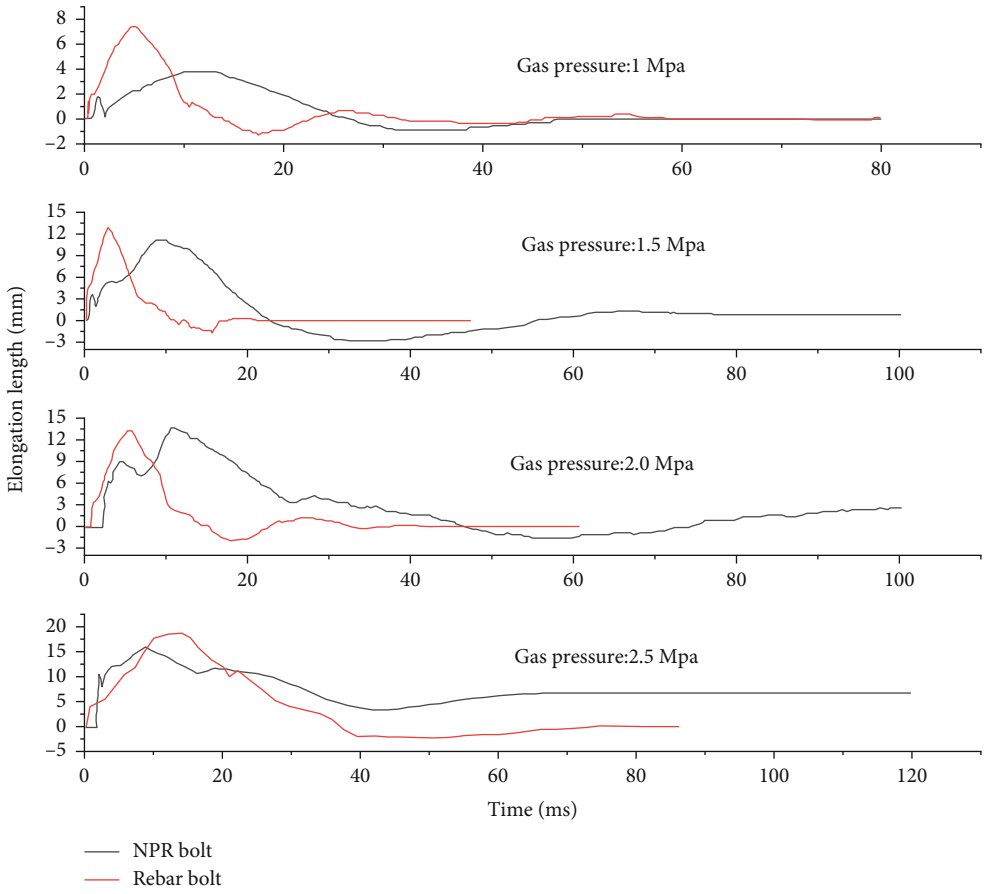

Figure 11: Elongation length-time curve for NPR and rebar bolt during impact process (wavelength: 1.4 m).

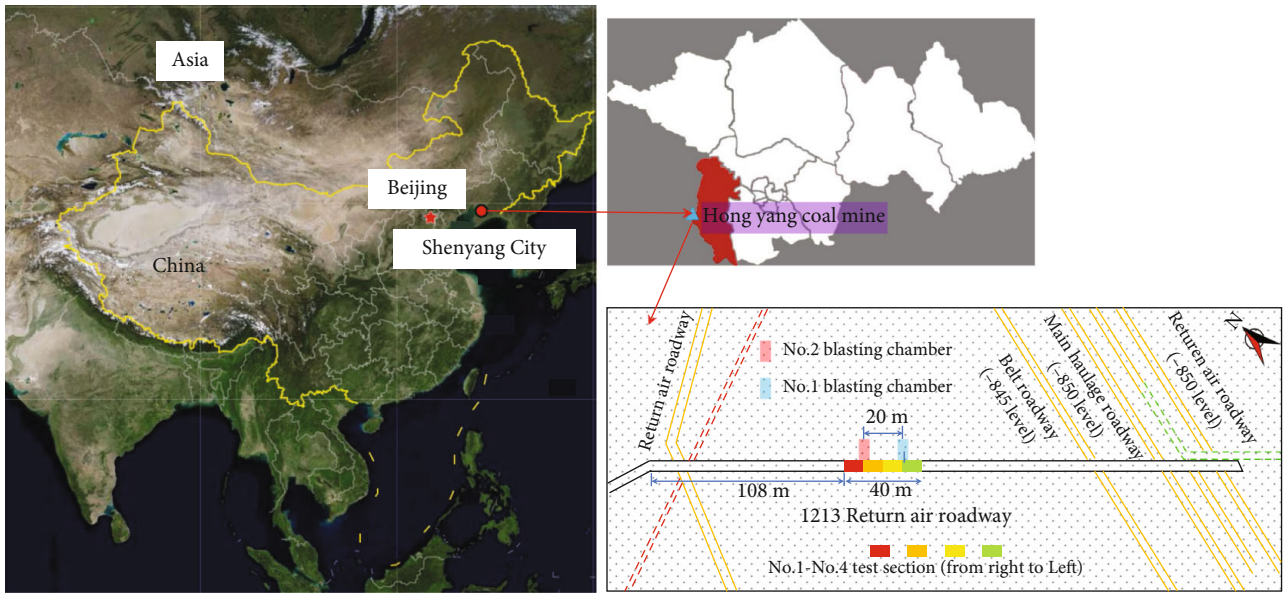

Figure 12: Position of Hongyang No. 3 Mine, Shengyang, China.

section was 3 m × 2.5 m (length × height), 4.5 m deep into the left coal wall. The roof and two sides were supported by a bolt-cable-metal mesh in the blasting chamber. Three φ20 mm × 2200 mm rebar bolts were installed on the roof, with row and column spacings of 800 and 800 mm, respectively. The metal mesh was created from 8# iron wire, with 70 mm × 80 mm mesh holes. The supporting section is shown in Figure 13.

Downloaded from http://pubs.geoscienceworld.org/gsa/lithosphere/article-pdf/doi/10.2113/2022/7057344/5681874/7057344.pdf
by guest

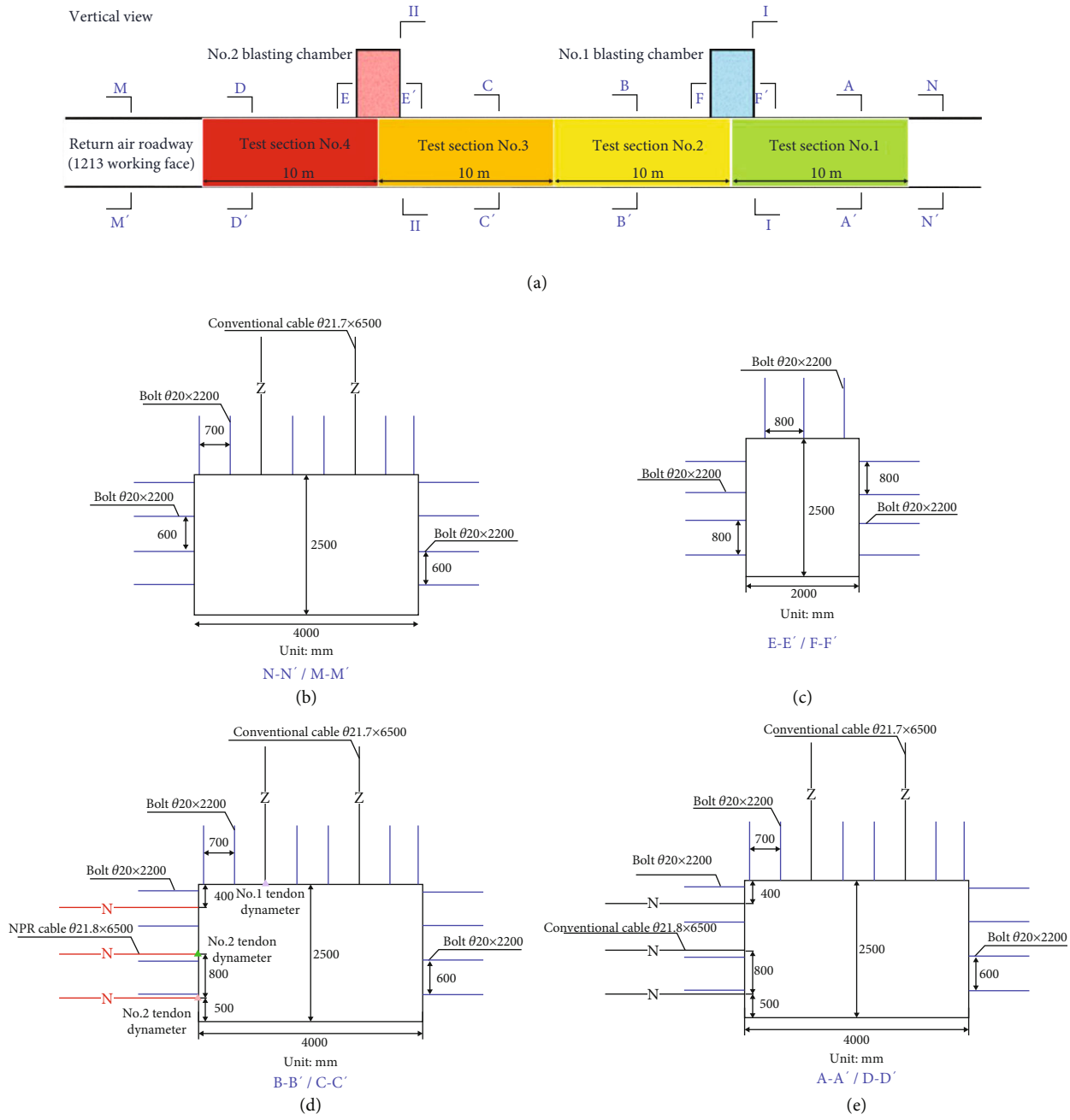

Figure 13: Support schemes of test sections.

4.2.3. Experimental Process. In the test, the blasting source was arranged in the interior of the blasting chamber, and the blasting hole was parallel to the roadway. The blasting impact test was preset 1-2 times in each test section. Test sections no. 1 and no. 3 are taken as examples.

(1) Test Section No. 1. Two blasting holes were arranged vertically in the blasting chamber, 1000 and 1700 mm away from the roof, respectively, and 2500 mm away from the roadway side. The upper hole length was 6.6 m with a charge of 4.4 kg, the lower hole length was 7.8 m with a charge of 6 kg, and the total charge was 10.4 kg (Figure 14(a)).

In test section no.3, two impact blasting tests were performed, and the cumulative charge was 30.4 kg. For the first time, three blast holes were arranged in the blasting chamber, 1000, 1300, and 1700 mm away from the roof, respectively (Figure 14(b)). The upper and lower blast holes were 3600 mm from the roadway side. The upper and lower blast holes were 5.2 m long, and each charge was 3.2 kg. The middle blast hole was 2500 mm away from the roadway side. The hole length was 7 m, and the charge was 5 kg. Three blast holes were simultaneously detonated. After the first blasting test in the no. 3 test section, the roadway was stable overall.

In the second blasting test, three vertical blast holes were arranged in the blasting chamber, which were 1000, 1500,

Downloaded from http://pubs.geoscienceworld.org/gsa/lithosphere/article-pdf/doi/10.2113/2022/7057344/5681874/7057344.pdf
by guest

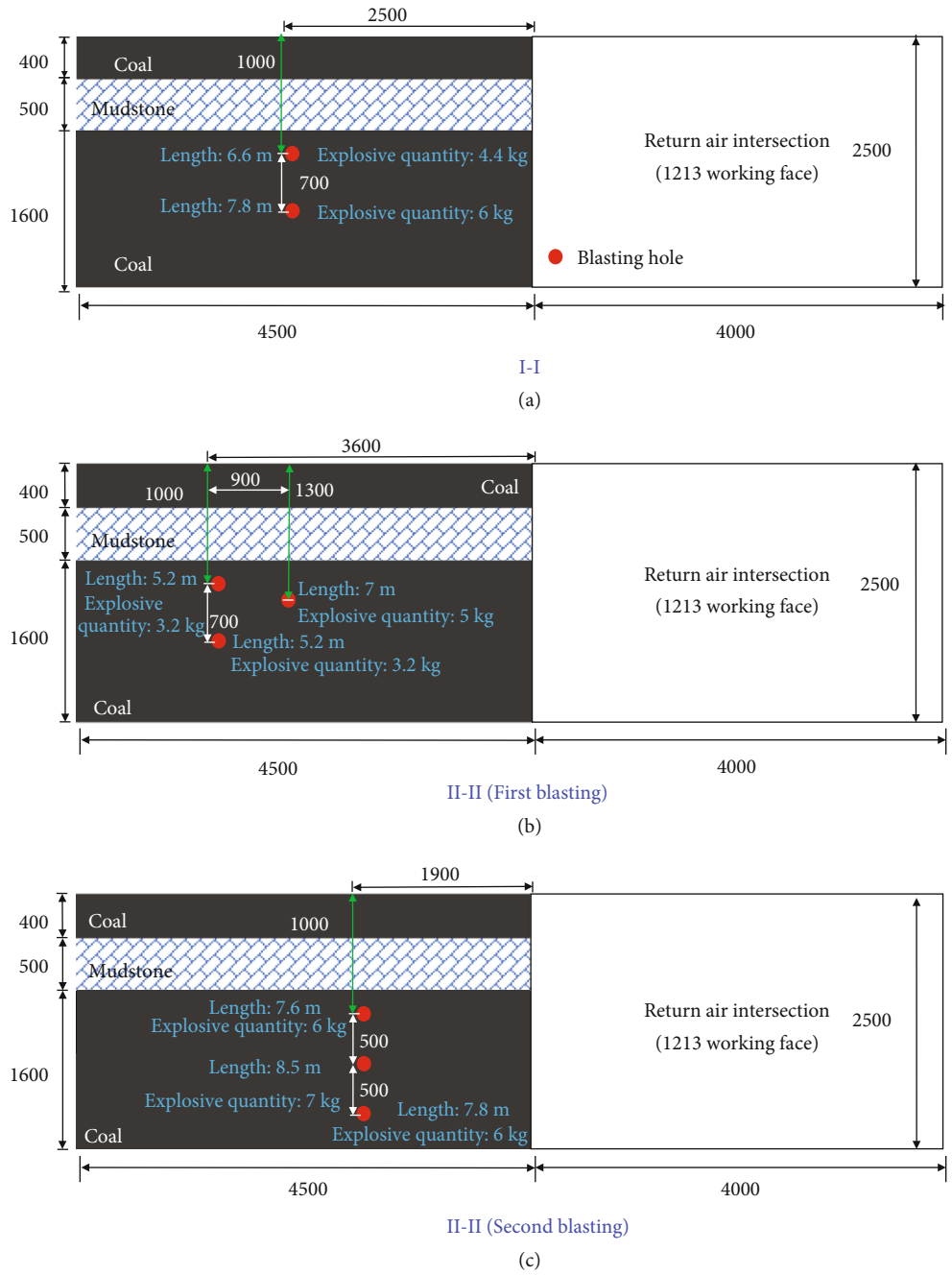

Figure 14: Scheme of blasting holes.

and 2000 mm away from the roadway roof, respectively, and 1900 mm away from the roadway side. The charge amounts of the three blast holes were 6, 7, and 6 kg, respectively, for a total of 19 kg. A single blasting was conducted (Figure 14(c)).

4.3. Results. Before blasting, test section no. 1 had a good support and overall stability (Figure 15(a)). After the blasting test, the roadway was unstable, and the sides were flushed out. Its width was approximately 6 m. The maximum depth of the crater was 1.8 m. The middle row of cables was pulled out, and some cables and bolts were pulled out and failed. The rock mass thrown out by the blasting shock was crushed, and the rock mass inside the crater was massive. The deformation of the rock surrounding the crater was small. The iron wire mesh was radially damaged around the crater, and the conventional cables were pulled out (Figures 15(b)–15(d)). The conventional cable contributed to controlling the deformation of the surrounding rock during the impact process. Because the cable and surrounding rock could not be coupled in terms of strength and stiffness, the cable support failed. This indicated that a conventional cable cannot adapt to the impact failure of the roadway surrounding rock and cannot effectively control the deformation of the surrounding rock under dynamic loads.

The test section no. 3 was well supported and stable overall before the blast test (Figure 16(a)). After the first

Downloaded from http://pubs.geoscienceworld.org/gsa/lithosphere/article-pdf/doi/10.2113/2022/7057344/5681874/7057344.pdf
by guest

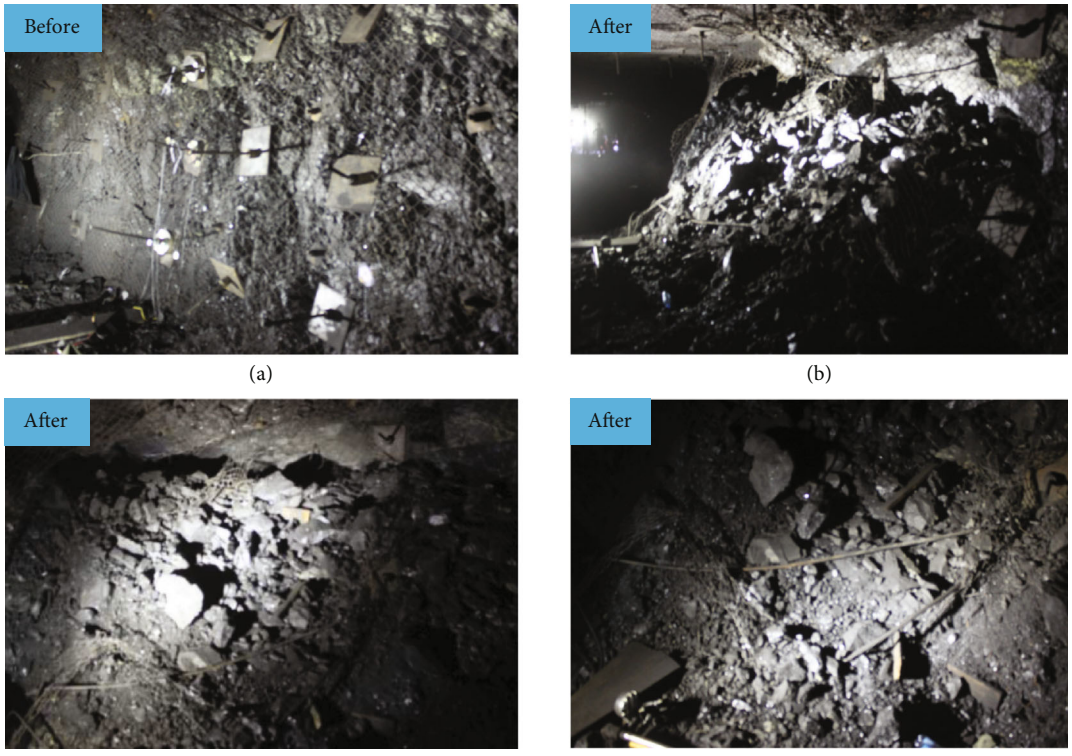

Figure 15: State of roadway in test section no. 1: (a) before blasting, (b) after blasting, (c) position of crater, and (d) cables pulled out.

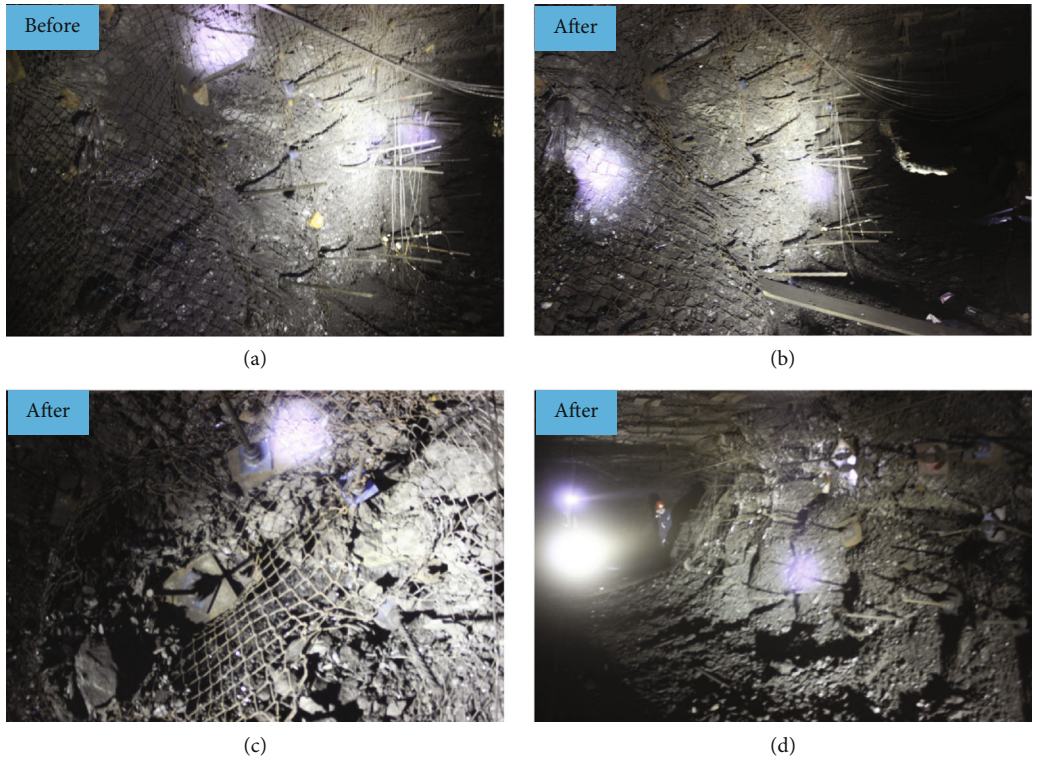

Figure 16: State of roadway in test section no. 3: (a) before blasting, (b) after blasting (first blasting), (c) small deformation of metal mesh (second blasting), and (d) roadway stability (second blasting).

Downloaded from http://pubs.geoscienceworld.org/gsa/lithosphere/article-pdf/doi/10.2113/2022/7057344/5681874/7057344.pdf
by guest

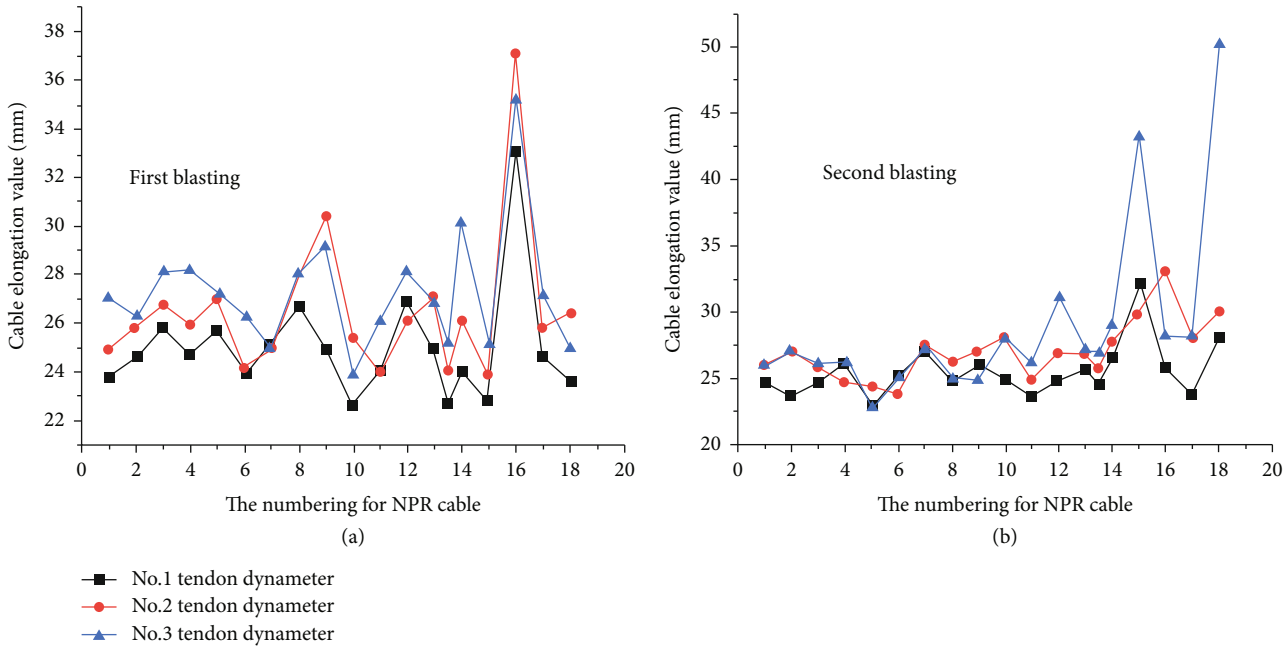

Figure 17: NPR cable elongation value.

blasting test, the roadway surface did not change significantly; however, the metal mesh around NPR cable deformed slightly (Figure 16(b)). After the impact test, the constant-resistance device experienced slipping. Most of the elongation of the NPR cable was between 20 and 30 mm, and the maximum elongation reached 38 mm (Figure 17(a)). The results indicated that the NPR cable generated a large deformation through the relative slipping between the constant resistance device and sleeve during the blasting shock, which adequately dissipated the energy generated by the rockburst. After the second blasting test, the overall roadway remained stable; however, the deformation of the metal mesh increased based on the first blasting (Figures 16(c) and 16(d)). In addition, the constant-resistance device further produced slip, and the maximum elongation of the NPR cable was 52 mm (Figure 17(b)).

5. Concluding Remarks

The dynamic response characteristics of NPR and rebar bolts under different impact wavelengths were studied using an NPR bolt impact tensile system, and a field test for simulating rockburst by blasting was designed and applied. The following conclusions were drawn:

(1) In the impact test, the NPR bolt only underwent constant resistance structural deformation, and the rod body was not broken. In contrast, the rebar bolt body was broken and exhibited necking

(2) The peak impact forces of the NPR and rebar bolts are inversely proportional to the wavelength. The shorter the wavelength, the faster the impact velocity and the higher the peak impact force. The maximum elongation of the bolt during the impact process is inversely proportional to the wavelength. The shorter the wavelength, the greater the peak value of elongation and the greater the amplitude of elongation and rebound

(3) Under the same impact wavelength, the impact force of the NPR bolt decays rapidly; after reaching the impact force peak, the number of impact force peaks and the peak is small. The peak value of the impact force of the rebar bolt is high, and the curve shows a multipeak phenomenon in the impact force response process without apparent rapid attenuation

(4) The field blasting method simulated the impact resistance performance of NPR and conventional cables. The test results showed that the conventional cable of the test section broke, and overall roadway collapse occurred. The NPR cable produced instantaneous slip deformation under the action of an explosion impact force, absorbed the impact energy generated by the explosion, and the test section roadway produced a limited and controllable deformation. The roadway was stable, indicating that the NPR cable had good impact resistance performance

Data Availability

All the data and models that support the findings of this study are available from the corresponding author upon reasonable request.

Conflicts of Interest

The authors declare that they have no known competing financial interests or personal relationships that could have appeared to influence the work reported in this paper.

Downloaded from http://pubs.geoscienceworld.org/gsa/lithosphere/article-pdf/doi/10.2113/2022/7057344/5681874/7057344.pdf
by guest

Acknowledgments

Funding for this work was provided by the National Natural Science Foundation of China (52074300), the National Natural Science Foundation of China Youth Science Foundation Project (52104139), and the State Key Laboratory for GeoMechanics and Deep Underground Engineering, China University of Mining and Technology, Beijing (SKLGDUEK2132).

References

[1] M. Z. Gao, B. G. Yang, J. Xie et al., "The mechanism of microwave rock breaking and its potential application to rock-breaking technology in drilling," *Petroleum Science*, vol. 19, no. 3, pp. 1110–1124, 2022.

[2] Z. Dou, S. Tang, X. Zhang et al., "Influence of shear displacement on fluid flow and solute transport in a 3D rough fracture," *Lithosphere*, vol. 2021, no. Special 4, article 1569736, 2021.

[3] C. Cao, W. Zhang, J. Chen, B. Shan, S. Song, and J. Zhan, "Quantitative estimation of debris flow source materials by integrating multi- source data: a case study," *Engineering Geology*, vol. 291, article 106222, 2021.

[4] Z. Dou, Y. Liu, X. Zhang et al., "Influence of layer transition zone on rainfall-induced instability of multilayered slope," *Lithosphere*, vol. 2021, no. Special 4, article 2277284, 2021.

[5] G. Li, Y. Hu, S. M. Tian, and H. L. Huang, "Analysis of deformation control mechanism of prestressed anchor on jointed soft rock in large cross-section tunnel," *Bulletin of Engineering Geology and the Environment*, vol. 80, no. 12, pp. 9089–9103, 2021.

[6] Y. Wang, C. H. Li, Y. Z. Hu, and X. L. Zhou, "A new method to evaluate the brittleness for brittle rock using crack initiation stress level from uniaxial stress–strain curves," *Environmental Earth Sciences*, vol. 76, no. 23, pp. 1–18, 2017.

[7] Y. Wang, W. H. Tan, D. Q. Liu, Z. Q. Hou, and C. H. Li, "On anisotropic fracture evolution and energy mechanism during marble failure under uniaxial deformation," *Rock Mechanics and Rock Engineering*, vol. 52, no. 10, pp. 3567–3583, 2019.

[8] W. Zhi-jun, F. Li-feng, L. Quan-sheng, and M. Guo-wei, "Micro-mechanical modeling of the macro-mechanical response and fracture behavior of rock using the numerical manifold method," *Engineering Geology*, vol. 225, pp. 49–60, 2017.

[9] W. U. Zhi-jun, X. U. Xiang-yu, L. I. U. Quan-shen, and Y. A. N. G. Yong-tao, "A zero-thickness cohesive element-based numerical manifold method for rock mechanical behavior with micro-Voronoi grains," *Engineering Analysis with Boundary Elements*, vol. 96, pp. 94–108, 2018.

[10] F. Guo-rui, B. Jin-wen, S. Xu-dong et al., "Key pillar theory in the chain failure of residual coal pillars and its application prospect," *Journal of China Coal Society*, vol. 46, no. 1, pp. 164–179, 2021.

[11] W. Blake, *Rockburst Mechanics*, Colorado School of Mines, Golden, 1967.

[12] F. Xia-ting, X. Ya-xun, F. Guang-liang et al., "Study on the development process of rockburst," *Chinese Journal of Rock Mechanics and Engineering*, vol. 38, no. 4, pp. 649–673, 2019.

[13] H. Bao-yu, *True Triaxial Test on Rockburst of Granites with Different Water Saturation*, Guangxi University, Nanning, 2018.

[14] M. Jiao-yang, *Research on the Rockburst Control Methods of Erdaogou Gold Mine*, Northeastern University, Shenyang, 2011.

[15] B. Zhao, *True-Triaxial Strainburst Test of Different Hard Rocks*, Guangxi University, Nanning, 2018.

[16] J. I. A. N. G. Fei-fei, H. Zhou, C. Liu, and J. Sheng, "Progress, prediction and prevention of rockbursts in underground metal mines," *Chinese Journal of Rock Mechanics and Engineering*, vol. 38, no. 5, pp. 956–972, 2019.

[17] X. Hu, G. Su, K. Chen, T. Li, and Q. Jiang, "Strainburst characteristics under bolt support conditions: an experimental study," *Natural Hazards*, vol. 97, no. 2, pp. 913–933, 2019.

[18] L. Chun-lin, "A new energy-absorbing bolt for rock support in high stress rock masses," *International Journal of Rock Mechanics and Mining Sciences*, vol. 47, no. 3, pp. 396–404, 2010.

[19] W. D. Ortlepp, "Yieldable rock bolts for shock loading and grouted bolts for faster rock stabilization," *The Mines Magazine, Colorado School of Mines*, vol. 60, no. 3, pp. 12–17, 1970.

[20] W. D. Ortlepp, "Considerations in the design of support for deep hard rock tunnels," in *Proceedings of the 5th Congress of the International Society for Rock Mechanics*, pp. D179–D187, Melbourne, Australia, 1983.

[21] T. F. Herbst, "Yieldable Roof Support for Mines," in *Proceedings of the 31st US Symposium*, pp. 807–814, Rotterdam and Brookfield, 1990.

[22] B. Stillborg, "Rockbolt and cablebolt tensile testing across a joint," in *Mining and Geotechnical Consultants*, Lulea, Sweden, 1990.

[23] X. M. Sun, D. Wang, C. Wang, X. Liu, B. Zhang, and Z. Q. Liu, "Tensile properties and application of constant resistance and large deformation bolts," *Chinese Journal of Rock Mechanics and Engineering*, vol. 33, no. 9, pp. 1765–1771, 2014.

[24] H. Chao-jiong, G. Li-sheng, and G. Pai-feng, "Bolting Support in Coal Roadway," China University of Mining and Technology Press, Beijing, 1999.

[25] G. Pai-feng, *Study on Improving Strength and Stability of Surrounding Rock by Bolt Support in Roadway*, China University of Mining and Technology, Xuzhou, 1998.

[26] W. D. Ortlepp, "Invited lecture: the design of support for the containment of rockburst damage in tunnels-an engineering approach," in *Proceedings of the International Symposium on Rock Support*, pp. 593–609, A.A. Balkema, Rotterdam, Netherlands, 1992.

[27] R. Varden, R. Lachenicht, J. R. Player, A. Thompson, and E. Villaescusa, "Development and Garford dynamic bolt at the Kanowna belle mine," in *Tenth Underground Operators Conference*, pp. 95–104, Australia, 2008.

[28] F. Charette and M. Plouffe, "A new rock bolt concept for underground excavations under high stress conditions," in *Proceedings of 6th International Symposium on Ground Support in Mining and Civil Engineering Construction*, pp. 225–240, Johannesburg, 2008.

[29] A. Ansell, "Dynamic testing of steel for a new type of energy absorbing rock bolt," *Journal of Constructional Steel Research*, vol. 62, no. 5, pp. 501–512, 2006.

[30] A. E. H. Love, *A Treatise on the Mathematical Theory of Elasticity*, Cambridge University Press, New York, 1944.

[31] A. J. Jager, "Two new support units for the control of rockburst damage," in *International Symposium on rock Support*, pp. 621–631, Netherlands, 1992.

Downloaded from http://pubs.geoscienceworld.org/gsa/lithosphere/article-pdf/doi/10.2113/2022/7057344/5681874/7057344.pdf
by guest

[32] M. H. Turner and J. R. Player, "Seismicity at big bell mine," in *Proceedings Massmin*, pp. 791–797, Melbourne, 2000.

[33] M. Cai, "Principles of rock support in burst-prone ground," *Tunnelling and Underground Space Technology*, vol. 36, pp. 46–56, 2013.

[34] L. St-Pierre, F. P. Hassani, P. H. Radziszewski, and J. Ouellet, "Development of a dynamic model for a cone bolt," *International Journal of Rock Mechanics and Mining Sciences*, vol. 46, no. 1, pp. 107–114, 2009.

[35] D. Gaudreau, A. Gendron, and J. P. Basque, "Apparatus and method for a yieldable tendon mine support," 2002, U.S. Patent 6, 390, 735.

[36] B. Simser, W. C. Joughin, and W. D. Ortlepp, "The performance of Brunswick Mine's rockburst support system during a severe seismic episode," *Journal of the South African Institute of Mining and Metallurgy*, vol. 102, no. 4, pp. 217–223, 2002.

[37] A. Ansell, "Laboratory testing of a new type of energy absorbing rock bolt," *Tunnelling and Underground Space Technology*, vol. 20, no. 4, pp. 291–300, 2005.

[38] U. Ozbay and E. Neugebauer, "In-situ pull testing of a yieldable rock bolt, ROOFEX," *Controlling Seismic Hazard and Sustainable Development of Deep Mines*, vol. 2, pp. 1081–1090, 2009.

[39] M. Cai and P. K. Kaiser, "Rockburst support reference book-volume I: rockburst phenomenon and support characteristics," *Laurentian University*, vol. 284, 2018.

[40] M. C. He, C. Li, W. L. Gong, J. Wang, and Z. Tao, "Support principles of NPR bolts/cables and control; techniques of large deformation," *Chinese Journal of Rock Mechanics and Engineering*, vol. 35, no. 8, pp. 1513–1529, 2016.

[41] M. He, W. Gong, J. Wang et al., "Development of a novel energy-absorbing bolt with extraordinarily large elongation and constant resistance," *International Journal of Rock Mechanics and Mining Sciences*, vol. 67, pp. 29–42, 2014.

[42] P. K. Kaiser, "From common to best practices in underground rock engineering," in *Rock Mechanics for Natural Resources and Infrastructure Development*, pp. 141–179, CRC Press, 2019.

[43] M. Sharifzadeh, J. Lou, and B. Crompton, "Dynamic performance of energy-absorbing rockbolts based on laboratory test results. Part I: Evolution, deformation mechanisms, dynamic performance and classification," *Tunnelling and Underground Space Technology*, vol. 105, article 103510, 2020.

[44] M. Sharifzadeh, J. Lou, and B. Crompton, "Dynamic performance of energy-absorbing rockbolts based on laboratory test results. Part II: role of inherent features on dynamic performance of rockbolts," *Tunnelling and Underground Space Technology*, vol. 105, article 103555, 2020.

[45] G. Knox, A. Berghorst, and B. Crompton, "The Relationship between the Magnitude of Impact Velocity per Impulse and Cumulative Absorbed Energy Capacity of a Rock Bolt," in *Proceedings of The Fourth Australasian Ground Control in Mining Conference Proceedings*, pp. 160–169, The Australasian Institute of Mining and Metallurgy, Sydney Australia, 2018.

[46] L. I. Chun-lin and C. Doucet, "Performance of D-bolts under dynamic loading," *Rock Mechanics and Rock Engineering*, vol. 45, no. 2, pp. 193–204, 2012.

[47] W. Ai-wen, G. Qian-shu, D. Lian-peng, P. Yi-shan, Z. Jian-zhuo, and C. Jian-qiang, "Static and dynamic performance of rebar bolts and its adaptability under impact loading," *Journal of China Coal Society*, vol. 43, no. 11, pp. 2999–3006, 2018.

[48] G. Knox and A. Berghorst, "Increased agility For the Research and Development of Dynamic Roof Support Products," in *Rock Dynamics-Experiments, Theories and Applications*, pp. 373–378, CRC Press, 2018.

[49] R. Masoudi and M. Sharifzadeh, "Reinforcement selection for deep and high-stress tunnels at preliminary design stages using ground demand and support capacity approach," *International Journal of Mining Science and Technology*, vol. 28, no. 4, pp. 573–582, 2018.

[50] L. Song and H. Shi-sheng, "Two-wave and three-wave method in SHPB data processing," *Explosion and Shock Waves*, vol. 4, pp. 368–373, 2005.

[51] Z. Wan-cheng, T. Chun-an, and Z. Yujun, *Dynamic Damage and Fracture Process of Deep Rock Mass*, Science Press, Beijing, 2014.

[52] R. Yang, Y. Li, D. Guo, L. Yao, T. Yang, and T. Li, "Failure mechanism and control technology of water-immersed roadway in high- stress and soft rock in a deep mine," *Mining Science and Technology*, vol. 27, no. 2, pp. 245–252, 2017.

[53] M. Rong-rong, *Study on Tensile Properties and Damage Evolution Mechanism of Coal Measures Sandstone under High Strain Rate*, China university of mining and technology, Xuzhou, 2018.

[54] Z. Qian-bin and J. Zhao, "Determination of mechanical properties and full-field strain measurements of rock material under dynamic loads," *International Journal of Rock Mechanics and Mining Sciences*, vol. 60, pp. 423–439, 2013.

[55] X. Kai-wen and W. Yao, "Dynamic rock tests using split Hopkinson (Kolsky) bar system - a review," *Journal of Rock Mechanics and Geotechnical Engineering*, vol. 7, no. 1, pp. 27–59, 2015.

[56] Y. Wang and F. Xiao, *Principle of Electric Gun*, National defense industry press, Beijing, 1995.

[57] Z. Zhou, X. Cai, D. Ma et al., "Water saturation effects on dynamic fracture behavior of sandstone," *International Journal of Rock Mechanics and Mining Sciences*, vol. 114, pp. 46–61, 2019.

[58] S. Xu, X. M. Zhang, F. Pan, and J. X. Zhang, "Analysis on the energy testing methods of industrial explosives," *Explosive Materials*, vol. 42, no. 1, pp. 1001–8352, 2013.

[59] S. Wang, B. Li, J. Yao et al., "Experimental investigation of rock breakage by a conical pick and its application to non-explosive mechanized mining in deep hard rock," *International Journal of Rock Mechanics and Mining Sciences*, vol. 122, article 104063, 2019.

Downloaded from http://pubs.geoscienceworld.org/gsa/lithosphere/article-pdf/doi/10.2113/2022/7057344/5681874/7057344.pdf
by guest